Deng, W, Zhang, G, Murphy, MF, Lilley, F, Harvey, DM and Burton, DR

Analysis of dynamic cantilever behavior in tapping mode atomic force microscopy.

Analysis of Dynamic Cantilever Behaviour in Tapping Mode Atomic Force Microscopy

Wenqi Deng, Guang-Ming Zhang*, Mark F. Murphy, Francis Lilley, David M. Harvey, David R. Burton

W.Deng@2011.ljmu.ac.uk, G.Zhang@ljmu.ac.uk, M.F.Murphy@ljmu.ac.uk, F.Lilley@ljmu.ac.uk, D.M.Harvey@ljmu.ac.uk, D.R.Burton@ljmu.ac.uk

General Engineering Research Institute, Liverpool John Moores University
Byrom Street, Liverpool L3 3AF

Corresponding author*: Guang-Ming Zhang
Telephone: +441512312113

Abstract: Tapping mode Atomic Force Microscopy (AFM) provides phase images in addition to height and amplitude images. Although the behaviour of tapping mode AFM has been investigated using mathematical modelling, comprehensive understanding of the behaviour of tapping mode AFM still poses a significant challenge to the AFM community, involving issues such as the correct interpretation of the phase images. In this paper, the cantilever's dynamic behaviour in tapping mode AFM is studied through a three dimensional finite element method. The cantilever's dynamic displacement responses are firstly obtained via simulation under different tip-sample separations and for different tip-sample interaction forces, such as elastic force, adhesion force, viscosity force and the van der Waals force, which correspond to the cantilever's action upon various different representative computer-generated test samples. Simulated results show that the dynamic cantilever displacement response can be divided into three zones: a free vibration zone, a transition zone and a contact vibration zone. Phase trajectory, phase shift, transition time, pseudo stable amplitude and frequency changes are then analysed from the dynamic displacement responses that are obtained. Finally, experiments are carried out on a real AFM system to support the findings of the simulations.

Key words: tapping mode AFM; dynamic response; phase shift; finite element

1. Introduction

Tapping mode atomic force microscopy (AFM) has become popular in the area of biology (Whited and Park, 2014, Kasas et al., 2013), as well as for investigations in polymers (Duvigneau et al., 2014) and semiconductor materials science (Diao et al., 2013, Buyukkose et al., 2009). Unlike other AFM techniques, it only makes intermittent contact with the sample, which largely reduces any potential surface damage to soft materials, like cells. In addition to providing topographical images, tapping mode AFM also outputs a phase image, which can provide high resolution information about the structure of the sample. The phase image is calculated from the phase difference between the driving voltage signal that is applied to the cantilever and the actual displacement response of the cantilever (Jalili and Laxminarayana, 2004).

In a real AFM system, when we carry out tapping mode imaging, we normally determine a set-point, which is the nominal stable amplitude of the tapping cantilever, in order to obtain the phase image. When the cantilever moves from one X-Y position to the next X-Y position during the mechanical scanning process, the vibration amplitude will change due to the height difference between the two positions upon a sample's surface. During the tapping process, the feedback mechanism would send a signal to the piezo actuator, which causes the cantilever to move upwards, or downwards, along the Z-axis until the stable amplitude reaches the pre-determined set-point. The choice of set-point has a significant impact upon the quality of the phase images that are produced (Wang et al., 2003). It was found that the phase images could reproduce detailed structure of the sample when the set-point was fixed at around half of the free vibration amplitude. When the set-point was fixed at a value that is close to the free vibration amplitude, then the phase images could reveal no sample structure at all. The set-point not only depends upon the tip-sample separation, but also upon the level of indentation of the tip into the sample. The indentation level depends upon the material properties of the test sample.

In tapping mode AFM, the first order resonant frequency in the flexural mode has a major impact upon the phase shift. It is generally accepted that the phase shift in free vibration mode is 90^0 when the cantilever is vibrated at its first order resonant frequency. If the driving frequency is below the first order resonant frequency, then the phase shift will be smaller than 90^0. Otherwise, the phase shift will be larger than 90^0. The phase shift changes rapidly around

the resonant frequency. Thus, the cantilever is usually vibrated at, or near to, its first order resonant frequency (Magonov et al., 1997).

Researchers have tried to investigate what factors contribute to the phase shift. It can be seen that these interaction forces are affected by many factors, including tip-sample separation, radius of the tip and also the Young's modulus, surface energy and viscosity of the sample. In other words, all of these factors may make some contributions to the phase shifts that comprise the phase image. Although many studies have been carried out in multiple attempts to interpret AFM phase images (García et al., 1998, Tamayo and García, 1997, García García et al., 1999), a clear definition remains elusive.

However, it is generally accepted that energy dissipation causes changes in phase shifts. A point mass model (Tamayo and García, 1996, Tamayo and García, 1997, Garcia et al., 2006, García García et al., 1999, García et al., 1998, Song and Bhushan, 2008, Pishkenari et al., 2011) has been proposed to investigate the behaviour of tapping mode AFM. Results showed that the phase shift is independent of the Young's modulus of the material; the phase shift only changes when energy dissipation occurs, such as is the case with adhesion hysteresis and viscosity (Song and Bhushan, 2006, Song and Bhushan, 2008).

In this paper, a 3D finite element method is proposed to further study the dynamic behaviour of tapping mode AFM. Phase trajectory, phase shift, transition time, pseudo stable amplitude and frequency changes are then analysed from the dynamic displacement responses that are obtained. In the end of this study, we should indentify how phase shift are affected by different interaction forces and provide potential guidance on how to select setpoint amplitude for real AFM experiment.

2. Theory

The dynamic behaviour of a cantilever system can be generally described using second order differential equation as given below:

$$M\ddot{d} + C\dot{d} + Kd = F_{ext} + F_{ts} \quad (1)$$

Where M, C, K represents the system mass, damping and stiffness matrix, respectively. F_{ext} is the external force acting on the cantilever, while F_{ts} is the tip sample interaction force. Many physical models (Song and Bhushan, 2008, Melcher et al., 2008) have been developed for

different tip-sample interaction forces, such as elastic deformation, adhesion, viscosity, and van der Waals force. In this paper, the elastic force, $F_{elastic}$, is calculated using Equation 2, as follows:

$$F_{elastic} = \frac{4}{3}E^*\sqrt{R}(-d_0 - d)^{\frac{3}{2}}, \qquad d < d_0 \tag{2}$$

Where, E^* is the effective stiffness, R is radius of the tip, d_0 is the initial tip-sample separation, and d is the dynamic displacement of the tip. The term $-d_0 - d$ is the indentation of the tip into the sample. The effective stiffness E^* between the tip and sample is calculated using the following Equation:

$$E^* = [(1 - \sigma_t^2)/E_t + (1 - \sigma_s^2)/E_s]^{-1}. \tag{3}$$

Where E_t and E_s are the Young's modulus of the tip and sample respectively, and where σ_t and σ_t are the respective Poisson's ratio of the tip and the sample. The Adhesion force is calculated as follows:

$$F_{adhesion} = -4\pi R\gamma, \qquad d < d_0 \tag{4}$$

Where, γ is the surface energy. The surface energy is assumed to be different when the AFM tip retracts from the sample surface, compared to what it was when it initially approached the surface, which leads to adhesion energy hysteresis. The viscosity force is defined as:

$$F_{viscosity} = -\eta\sqrt{R(-d_0 - d)}\dot{d}, \qquad d < d_0 \tag{5}$$

Where, η is the viscosity, and $\dot{d}$ is the velocity in the normal direction. The van der Waals force is divided into two regions. When $-d_0 - d$ is larger than the intermolecular distance a_0, the van der Waals force is defined as:

$$F_v = -HR/6(-d_0 - d)^2 \tag{6}$$

Where H, R, d represent the Hamaker constant, radius of the tip and the instantaneous tip sample separation, respectively. When $-d_0 - d$ is smaller than a_0, the $-d_0 - d$ term is

substituted by a_0. In this case, the van der Waals force is then expressed as:

$$F_{vdW} = -HR/6a_0^2 \quad (7)$$

The definition of intermolecular distance is described as below:

$$a_0 = \sqrt{H/24\pi\gamma} \quad (8)$$

Where γ is the surface energy of the sample.

3. Finite element analysis of tapping mode AFM

The dynamic behaviour of a cantilever system is normally studied by solving Equation 1 using the Runge-Kutta algorithm. In this paper, the dynamic behaviour of the cantilever in tapping mode AFM is studied using the commercial COMSOL Multiphysics finite element modelling software. In finite element modelling, the cantilever is simulated as a linear elastic model coupled with non-linear interaction forces. The geometrical model of the cantilever system is shown in Figure 1. A fixed constraint is applied to the bottom surface of the virtual piezo actuator so that the piezo cannot move up and down; as a result the feedback system in the real AFM system is not modelled. In this study, we focus on the dynamic behaviour of the cantilever under the configuration depicted in Figure 1 rather than the popular bistable behaviour (Bahrami and Nayfeh, 2013) that is often studied by taking into account the AFM feedback system.

A computer-generated rectangular silicon cantilever with the following dimensions was used in the simulation, with dimensions of 240 μm length, 30 μm width, 2.7 μm thickness and with a silicon tip radius of 9nm. The cantilever dimensions are the same as those of the Olympus model AC240TS cantilevers which are typically used in our AFM experiments. The material properties of the silicon cantilever as used in the simulation again match those of the real cantilevers and are defined as: Young's modulus of 170 GPa and a Poisson's ratio of 0.28. A simulated piezo actuator with dimensions of 60 μm length, 30 μm width and 2 μm thickness is attached to the cantilever. A sinusoidal voltage signal is subsequently applied to the piezo actuator in order to vibrate the cantilever.

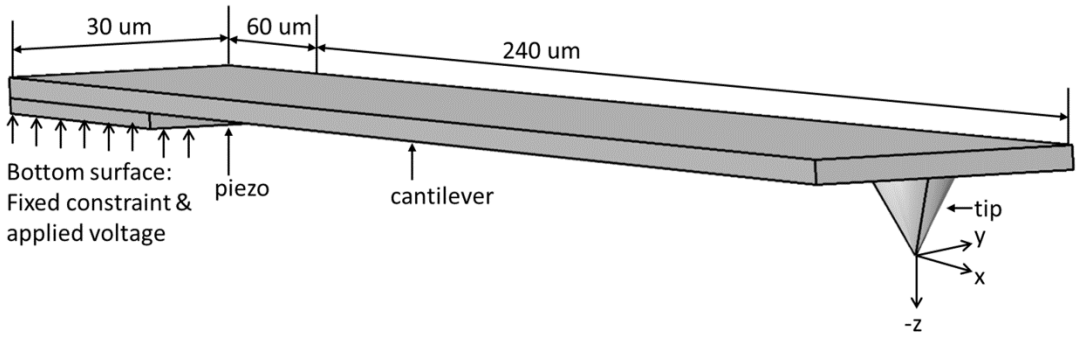

Figure 1 Geometric model of the cantilever

Modal analyses were firstly carried out for the cantilever shown in Figure 1. Different modes, such as the flexural mode, torsional mode, lateral bending mode and extensional mode were observed. The first resonant frequency of the cantilever is computed as 62,920 Hz on flexural mode which is widely used in tapping mode AFM.

In the proposed simulation model, no test sample is simulated. The tip-sample interaction is simulated by applying interaction forces to the AFM cantilever tip in the Z-axis, as is shown in Figure 1. The interaction forces including the elastic force, adhesion force, viscosity force, and the van der Waals force between the tip and the sample are defined in the simulation by the equations described in Section 2. The tip-sample contact position is determined by the tip-sample separation, as illustrated by the horizontal line in Figure 2. Moreover, in order to include adhesion energy hysteresis, the contact region is divided into two parts. When the tip reaches the horizontal line and enters region I, the contact force and adhesion force are taking effect. However, when the tip reaches the valley and begins to lift off, shown in region II, the adhesion energy changes. The difference between the approaching surface energy in region I and the retracting surface energy in region II would lead to energy dissipation, which is representative of the real world situation during experiments with an AFM instrument.

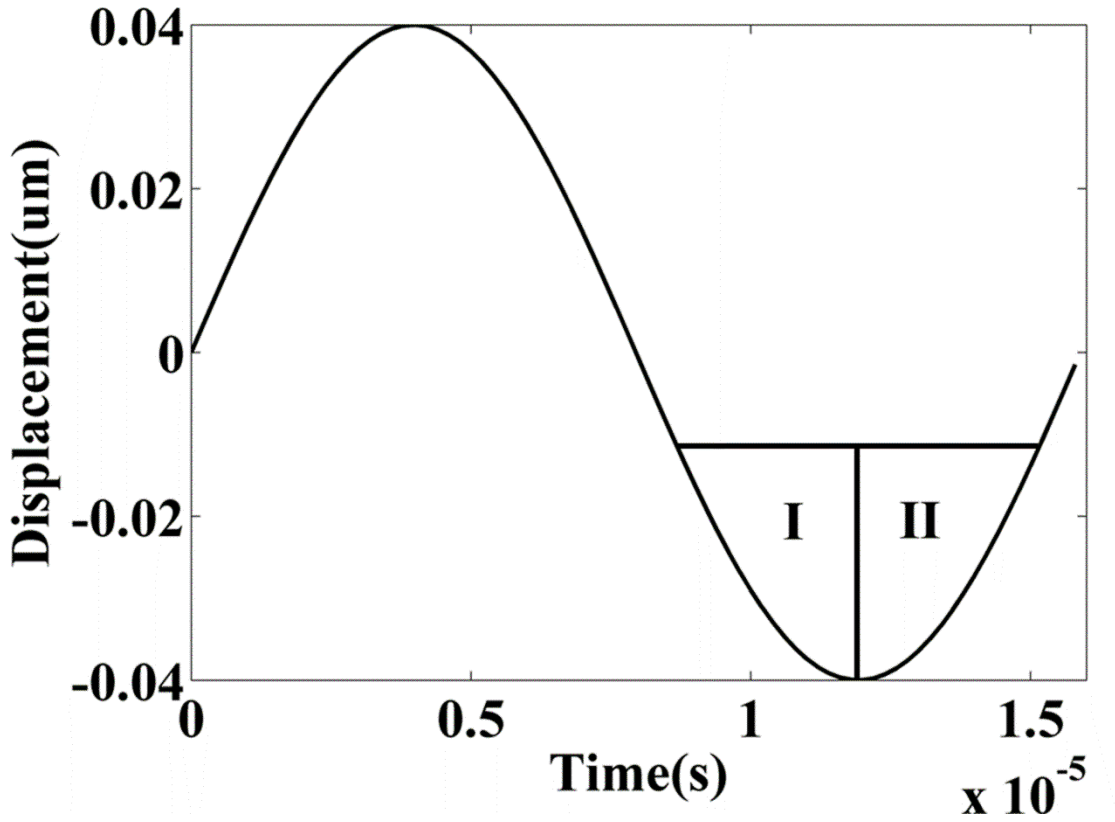

Figure 2 Illustration of tip-sample contact area with Free vibration amplitude Amp_{free}= 40nm and initial tip-sample separation d_0= 10nm. I: the approaching contact region; II: the retracting contact region.

In a real AFM experiment, the tip-sample separation is not measured. As mentioned earlier, the bottom of the piezo is fixed. Hence, in the proposed FEA method, we set the tip-sample separation, instead of the set-point, to study the dynamic behaviour of the cantilever during the tapping process in an X-Y position. Figure 3a shows a dynamic displacement response of the cantilever tapping a test sample. In the simulation, the cantilever starts from free vibration and then interacts with a test sample. From Figure 3a, it can be seen that the dynamic vibration of the cantilever can be divided into three zones: a free vibration zone, a transition zone, and a contact vibration zone that other modelling methods cannot observe. As mentioned above, the tip-sample interaction is simulated by applying different interaction forces between the tip and sample. The dynamic displacement response is obtained by only considering the elastic force using the following parameters: a resonant frequency of 62,920Hz, free vibration amplitude of 40nm, initial tip-sample separation, d0, of 20nm, a Young's modulus of the test sample of 1GPa, a Poisson's ratio of the test sample of 0.4, and a Q factor of 100. The Q factor indicates the experimental environment. Generally, the value for the Q factor in air lies between 100 to 200. In liquid, the Q factor usually ranges from 1 to 3. Notice that the Q factor has a significant impact upon the dynamic vibration of the

cantilever. Figure 3b shows the dynamic cantilever displacement response that is obtained by changing only the Q factor to a value of 1, compared to the previous value of Q = 100, that was shown previously in Figure 3a. It should be noted that the dynamic cantilever displacement response obtained in Figure 3b did not actually consider a discrete analysis of the fluid interaction upon the cantilever. Instead, the environment surrounding the cantilever is modelled and represented by the Q factor. The Q factor is related the damping ratio ζ as is shown in Equation 9.

$$Q = 1/2\zeta \tag{9}$$

Where the damping ratio ζ is one of the factors used to determine the damping coefficients, as Rayleigh damping (Liu and Gorman, 1995) is used to define the damping of the model. In other words, the Q factor has its own contribution in terms of determining the damping of the model. The definition of Rayleigh damping is shown in Equation 10.

$$C = \eta M + \delta K \tag{10}$$

Where C, M, K represents the matrices of the damping, mass and stiffness, respectively. The term η is the damping coefficient of the mass matrix, while δ is the damping coefficient of stiffness matrix. It is obvious that these two damping coefficients are important factors in Rayleigh damping. The damping coefficients are related the damping ratio ζ and the angular resonant frequencies w_i ($2\pi f_i$) and w_j ($2\pi f_j$) of the cantilever, as shown in Equations 11 and 12. The selection of the resonant frequencies determines the damping response of the system. In this study, the cantilever is vibrated at its first order flexural mode, thus we have chosen the first order and second order resonant frequencies of the cantilever's flexural mode for w_i and w_j respectively.

$$\delta = \frac{2\zeta}{w_i + w_j} \tag{11}$$

$$\eta = w_i w_j \delta \tag{12}$$

From Figure 3, it can be seen that a bigger Q factor leads to a larger transition zone (zone II).

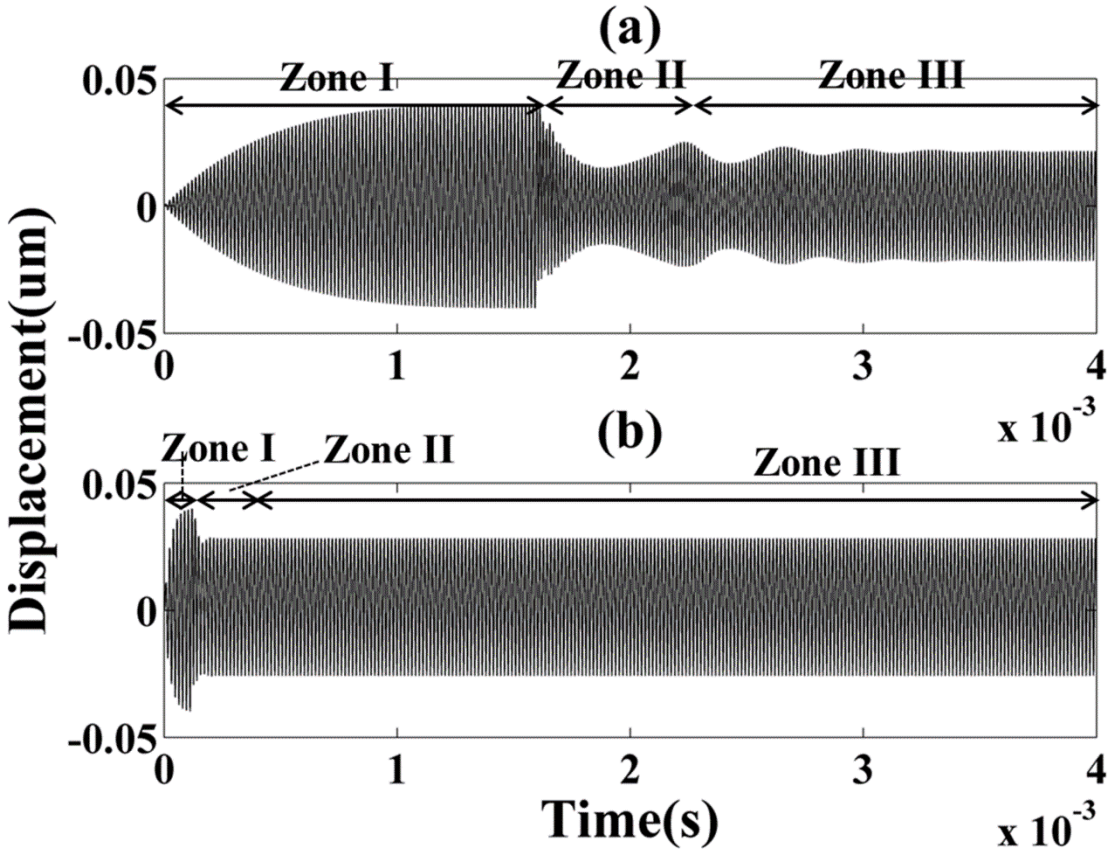

Figure 3 The simulated dynamic displacement response of a cantilever during tapping mode imaging when only considering the elastic force. Free vibration amplitude Amp_{free}= 40nm, tip-sample separation d_0= 20nm. Test sample material: Young's modulus of the test sample 1GPa, Poisson's ratio of the test sample 0.4. (a) Q=100. (b) Q=1.

4. Analysis of cantilever's dynamic behaviour

The cantilever's dynamic behaviour, such as phase trajectory, phase shift, transition time, stable amplitude, and vibration period changes, can then be subsequently analysed using the previously obtained dynamic displacement responses. These behaviours can help us to understand the phase images and may also enable us to optimize tapping mode AFM imaging.

4.1 Phase trajectory

Phase trajectory, which is defined as the relationship between the tip displacement and tip velocity, is an invaluable tool for use in studying dynamic systems. The phase trajectories for the three different zones in the displacement response that is shown in Figure 4a have been

plotted in Figures 5a to 5c respectively. Figures 5d to 5f show the corresponding phase trajectories for the second displacement response that was shown in Figure 4b with a larger initial tip-sample separation. The two different displacement responses shown in Figure 4 were obtained under the following parameters: initial tip-sample separations of 8nm (Figure 4a) and 20nm (Figure 4b), elastic force with Young's modulus of 1GPa and a Poisson's ratio of 0.4, and adhesion forces with an approach surface energy of 100mJ/m^2 and a retract surface energy of 150mJ/m^2. From Figure 5, it can be seen that the initial tip sample separation has significant impact on the behaviour of the phase trajectory during contact vibration, especially in Zone II. The trajectory in Zone II is very complicated. Figure 6 shows a few phase trajectories in different time positions within Zone II whose temporal positions are labelled using black arrows in Figure 4. It can be seen that the phase trajectory changes rapidly in Zone II. A physical explanation of the complex dynamic behaviour exhibited within Zone II needs further study in the future. Power spectrums of the displacements in Zone I, Zone II and Zone III are presented in Figure 7. When there is no tip sample interaction, as represented in Figures 7a and 7d, the vibration can be seen to be purely harmonic. On the other hand, higher harmonics occur when tip sample interaction forces are applied upon the tip, which are indicated by the cases shown in Figures 7(b-c) and 7(e-f).

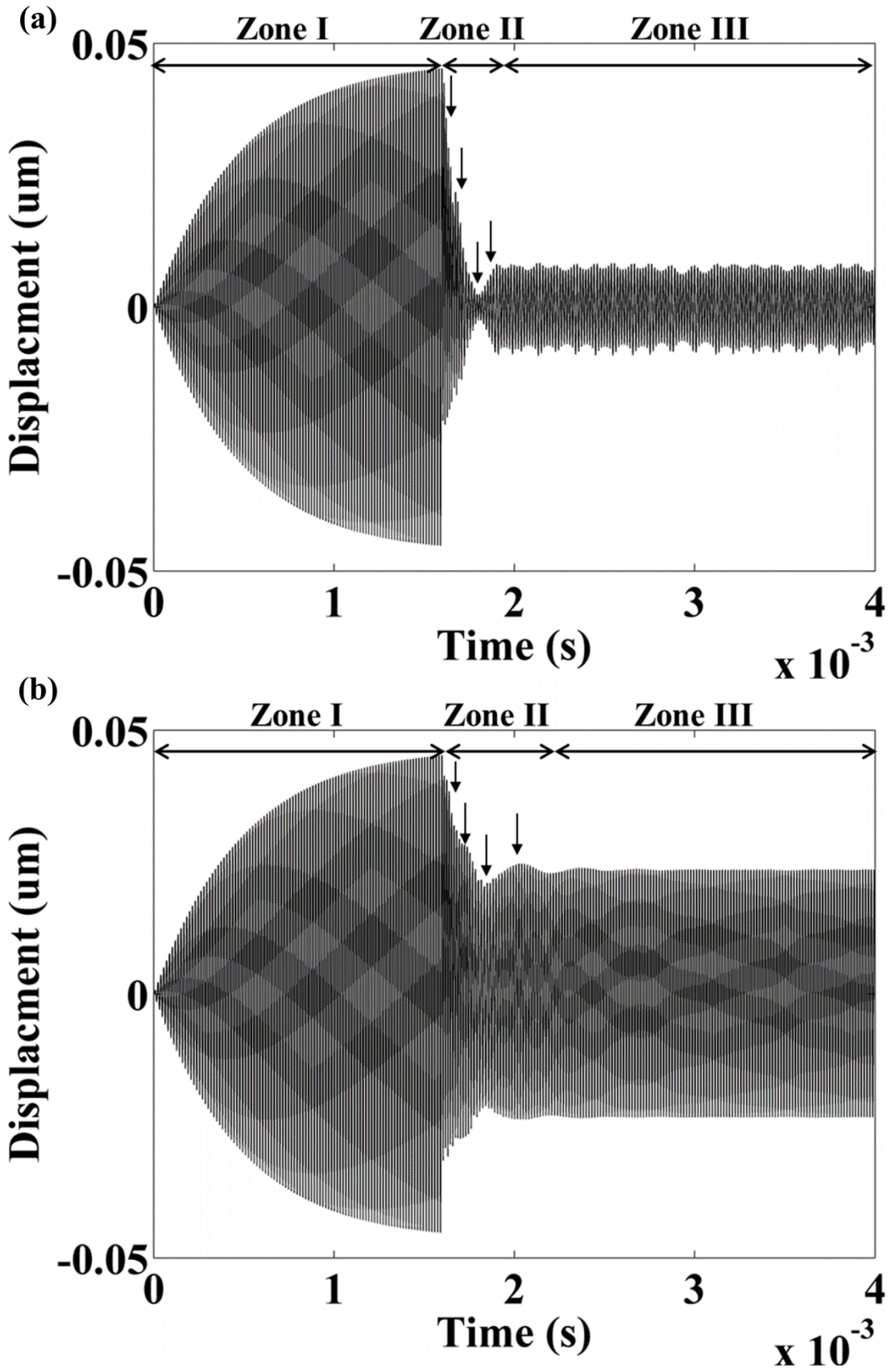

Figure 4 Two cantilever displacement signals at different initial tip-sample separations of (a) 8nm, (b) 20nm.

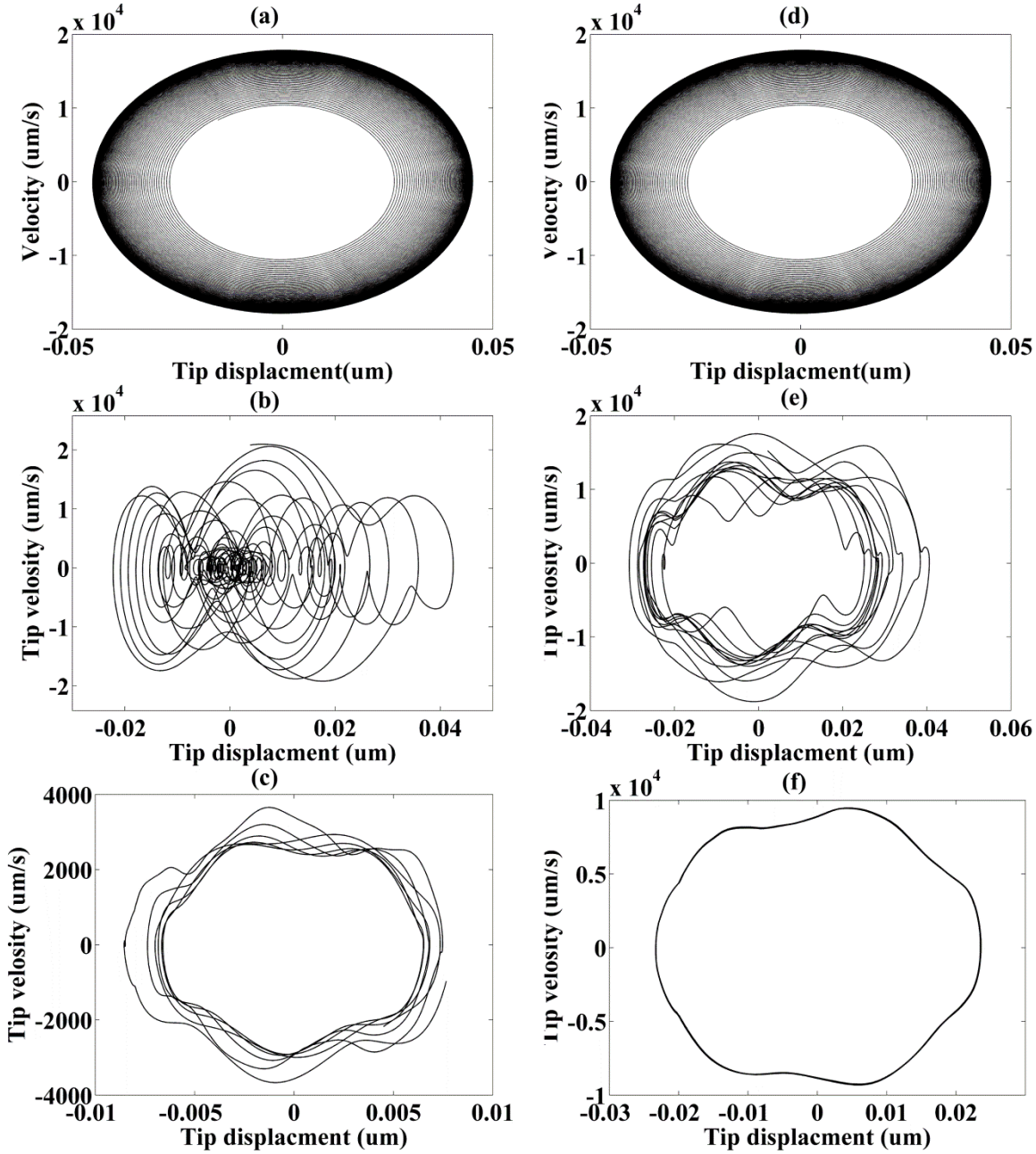

Figure 5 Phase trajectory of two cantilever displacements corresponding to Zone I (a,d), Zone II (b,e), Zone III (c,f)

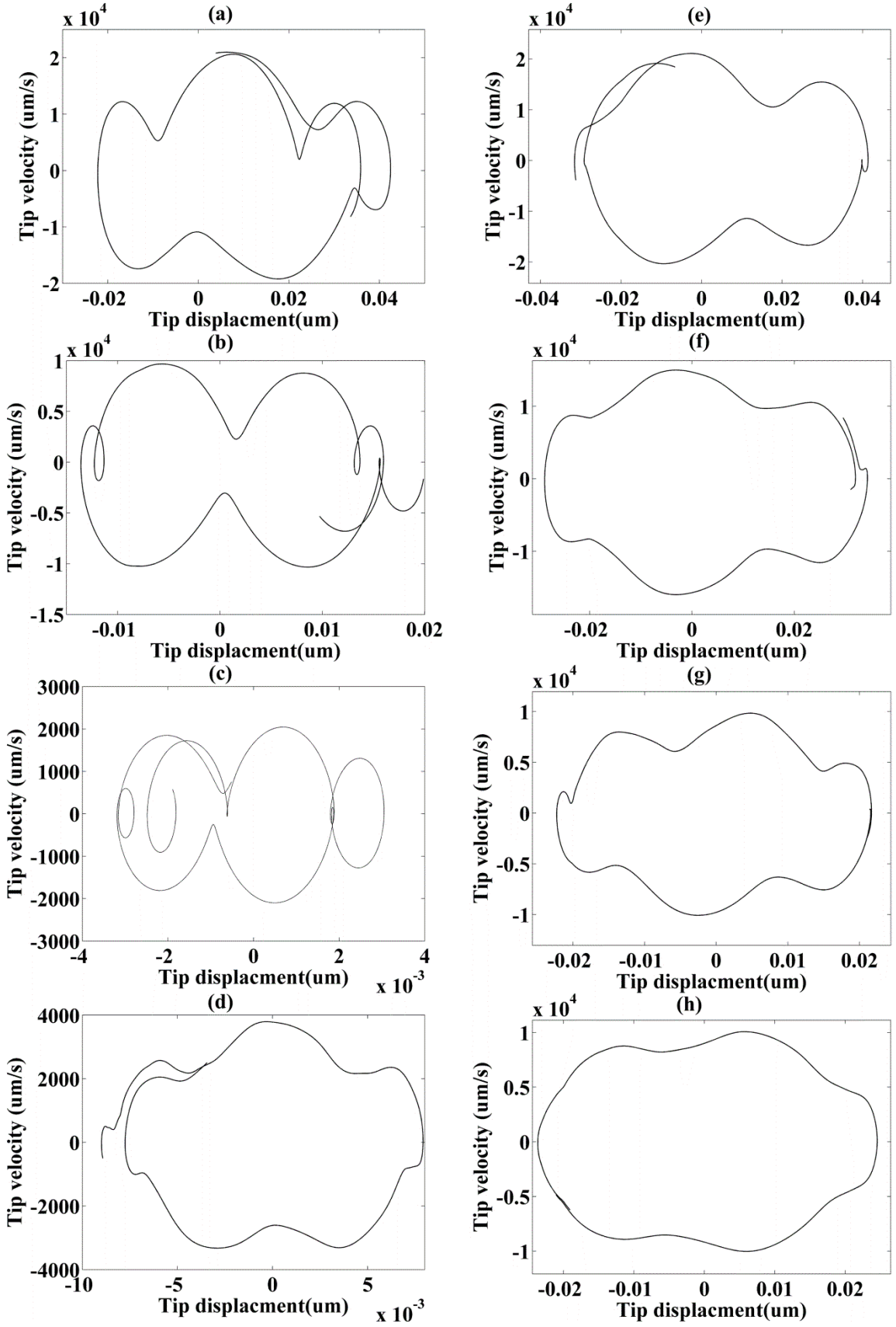

Figure 6 Phase trajectories at four discrete time intervals in Zone II (as defined by the black arrows in Figure 4) for initial tip sample separations of 8nm: (a-d) and 20nm: (e-h)

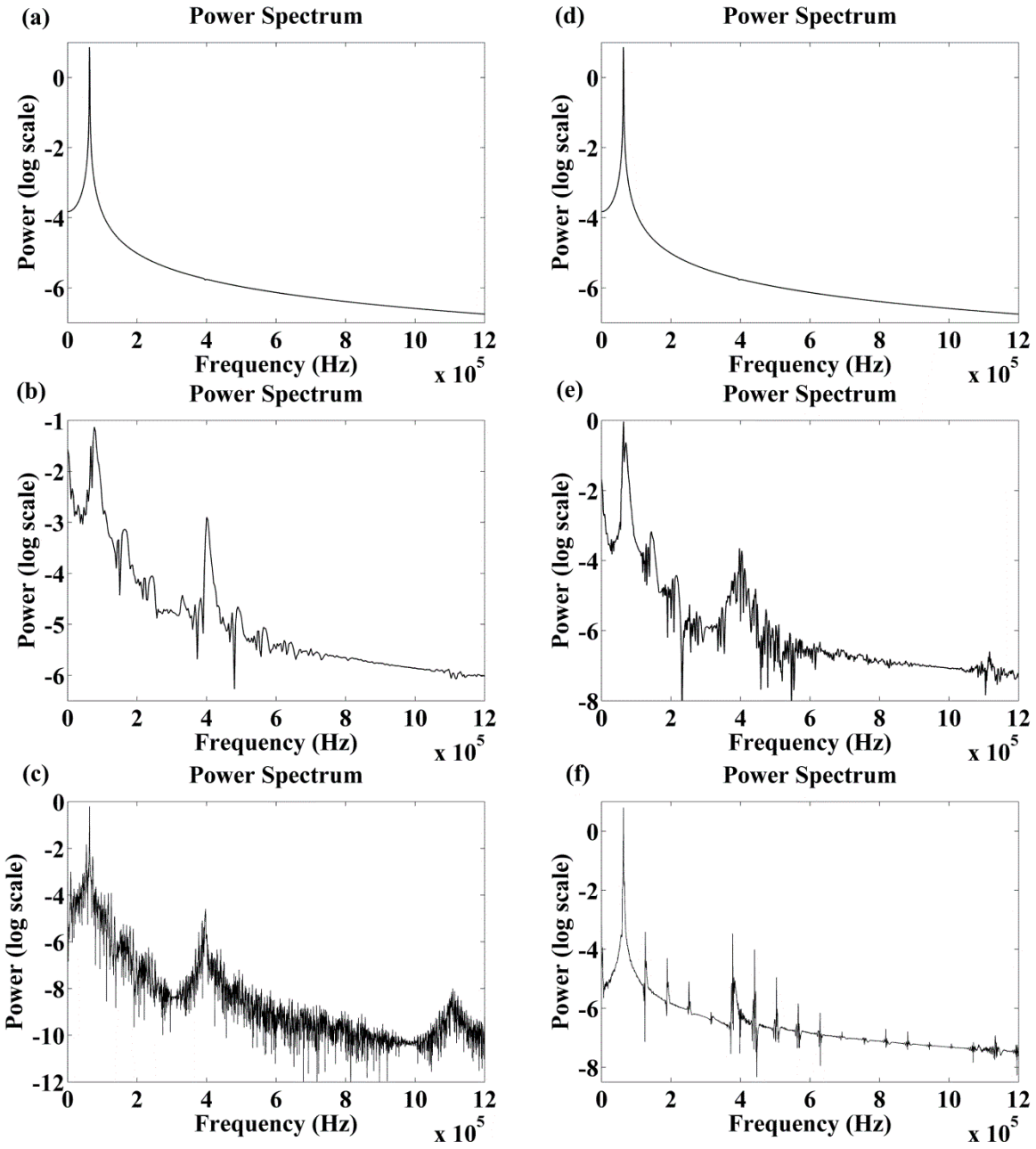

Figure 7 Power spectrums obtained from the entire displacement signals in Zone I (a,d); Zone II (b,e); Zone III (c,f) in Figure 4.

4.2 Phase shift

Phase shift is interpreted as being the phase lag between the driving voltage signal and the actual displacement response of the cantilever. A Fourier transform is first applied to the displacement response signal. Power spectrum and phase vs frequency curves then are obtained. Firstly, the frequency corresponding to the maximum power in the power spectrum

is established. Secondly, the phase angle that corresponds to this frequency is determined. The same method is subsequently applied to the voltage signal, rather than the displacement response signal. The difference between the phase angle of the displacement response signal and that of the voltage signal is then defined as representing the phase shift. This method for calculating the phase shift has been employed in all of the following results.

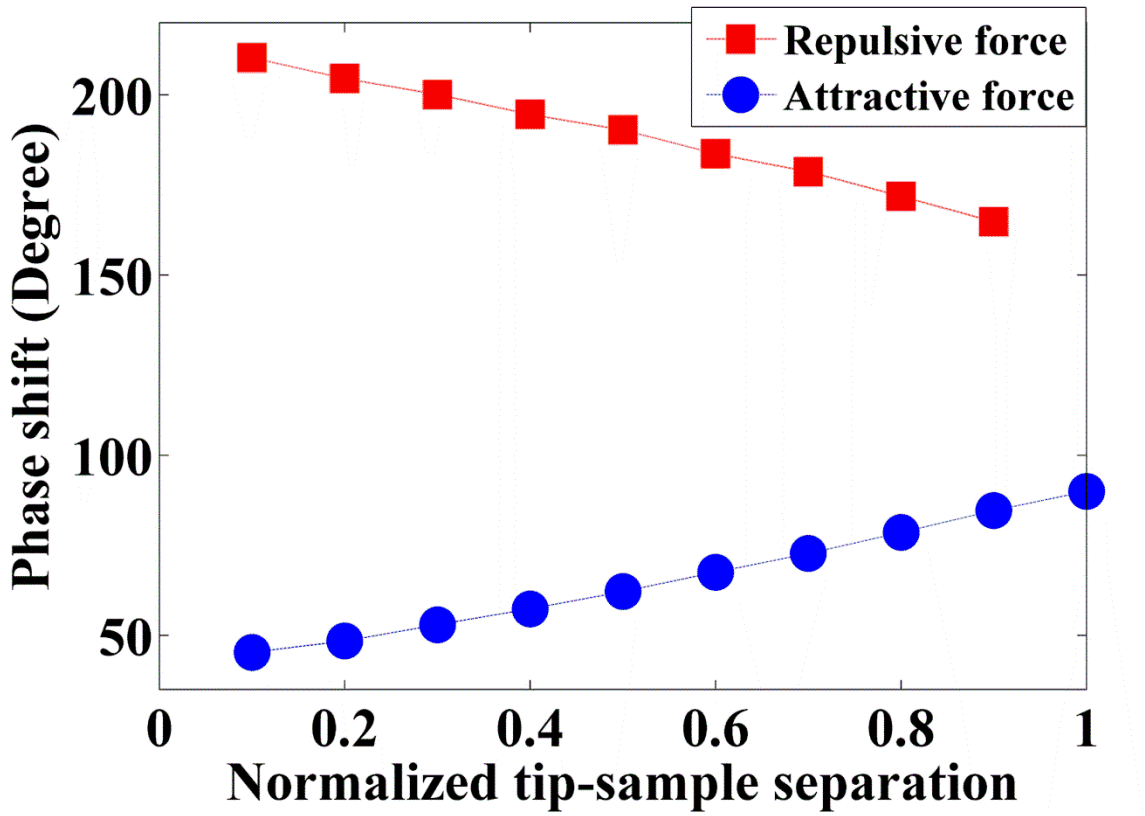

Figure 8 The trend of phase shifts when only elastic force or adhesion force is applied to the cantilever tip. Key: Square: elastic force; Circle: adhesion force. (Colour version: web only)

Figure 8 shows the behaviour of phase shifts when only the elastic force, or adhesion force, is applied to the tip surface in the Z-axis. The elastic force is defined here with a Young's modulus of 1GPa and a Poisson's ratio of 0.4, by using Equation 1. In addition identical approaching and retracting surface energies of 30 mJ/m^2 are used here to define the adhesion force. Notice that an offset is added into the phase shifts here to make the phase shift of the cantilever at free vibration equal to 90^o. This operation is always used in the real phase images produced by an actual tapping mode AFM system and so it is reproduced here and applied throughout the paper. The tip-sample separation d_0 is normalized to the cantilever's free vibration amplitude Amp_{free}:

$$d_{0n} = \frac{d_0}{\text{Ampfree}} \tag{13}$$

The normalized tip-sample separation d_{0n} is used to analyse the simulation results in this paper. As it can be seen in Figure 8, the phase shifts increase linearly as the tip-sample separation decreases (i.e., the tip is closer to the sample) shown in curve I when only elastic force is considered. On the other hand, the phase shifts decrease linearly as the tip-sample separation decreases shown in curve II when only adhesion force is considered. It is worth noting that the elastic force is a purely repulsive force and that the adhesion force is a purely attractive force. From Figure ~~6~~8, it can also be seen that the phase shifts are below 90° in the attractive regime, while the phase shifts are above 90° in the repulsive regime, which can be a potential indicator to analyse the phase shift when both repulsive and attractive forces are coupled into the simulation.

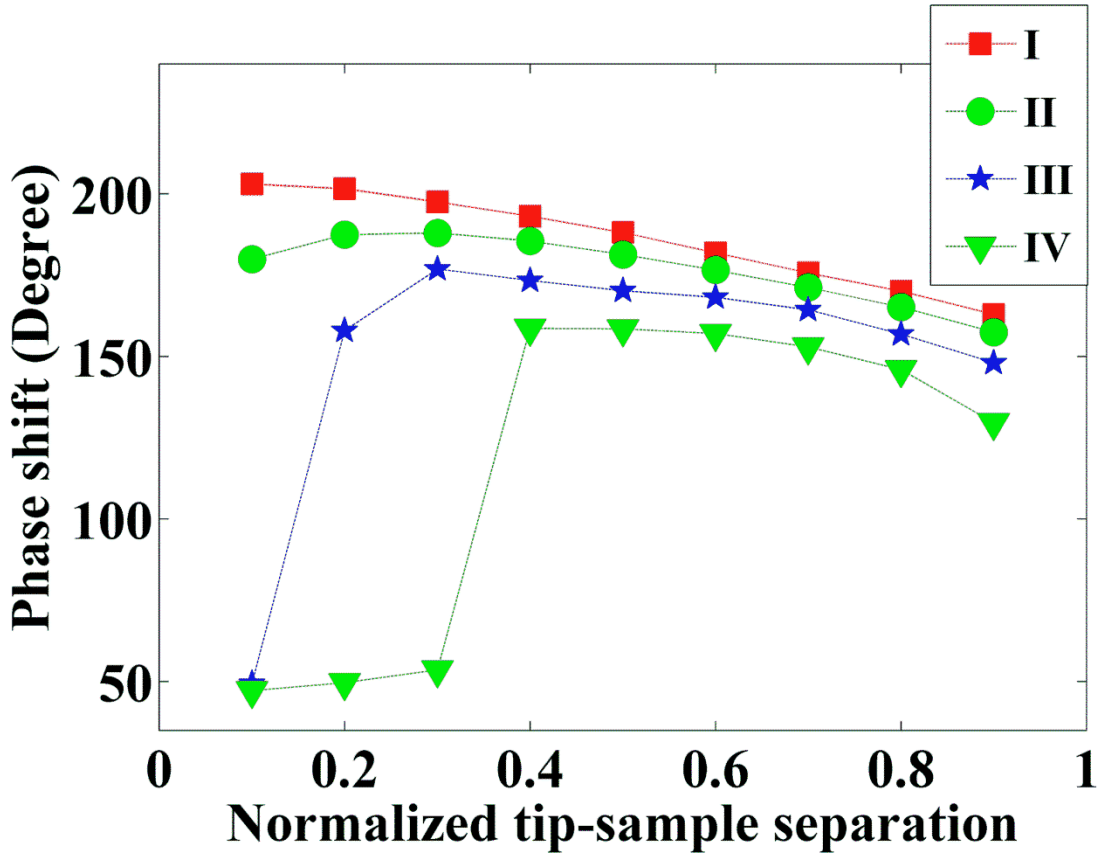

Figure 9 Phase shifts under elastic force and with different levels of adhesion energy hysteresis. The surface energy $\gamma_{approach}$ is 30mJ/m^2; The $\gamma_{retract}$ is respectively, 35mJ/m^2 (I), 60mJ/m^2 (II), 90mJ/m^2 (III), and 120mJ/m^2 (IV). (Colour version: web only)

Figure 9 shows the phase shifts under different levels of adhesion hysteresis, coupled with the elastic force, which are applied to the cantilever tip in the Z-axis. The elastic force is defined here with a Young's modulus of 1GPa and a Poisson's ratio of 0.4, by using Equation 1. In

curves I, II, III, IV, the approach surface energy $\gamma_{approach}$ is 30mJ/m^2, while the corresponding retract surface energies $\gamma_{retract}$ are 35mJ/m^2, 60mJ/m^2, 90mJ/m^2 and 120mJ/m^2, respectively. From Figure 9, it can be seen that the adhesion energy hysteresis decreases the phase shift significantly. For curves I and II, both are in the repulsive regime for all the tip-sample separations, but the phase shifts show a decreasing trend when the tip approaches the sample. When the level of hysteresis further increases, as in curve III, this shows a transition from the repulsive regime to the attractive regime as the tip-sample separation becomes smaller. It can be seen that in curve III the phase shift at a normalised tip-sample separation of 0.1 is below 90^o. This behaviour is more obvious when the level of hysteresis is further increased, as in curve IV, which shows that phase shifts are affected by the strength of the hysteresis. The transition from the repulsive regime into the attractive regime as the tip approaches the sample is due to the two opposite contributions to the phase shifts by the repulsive and attractive forces, as can be seen in Figure 8.

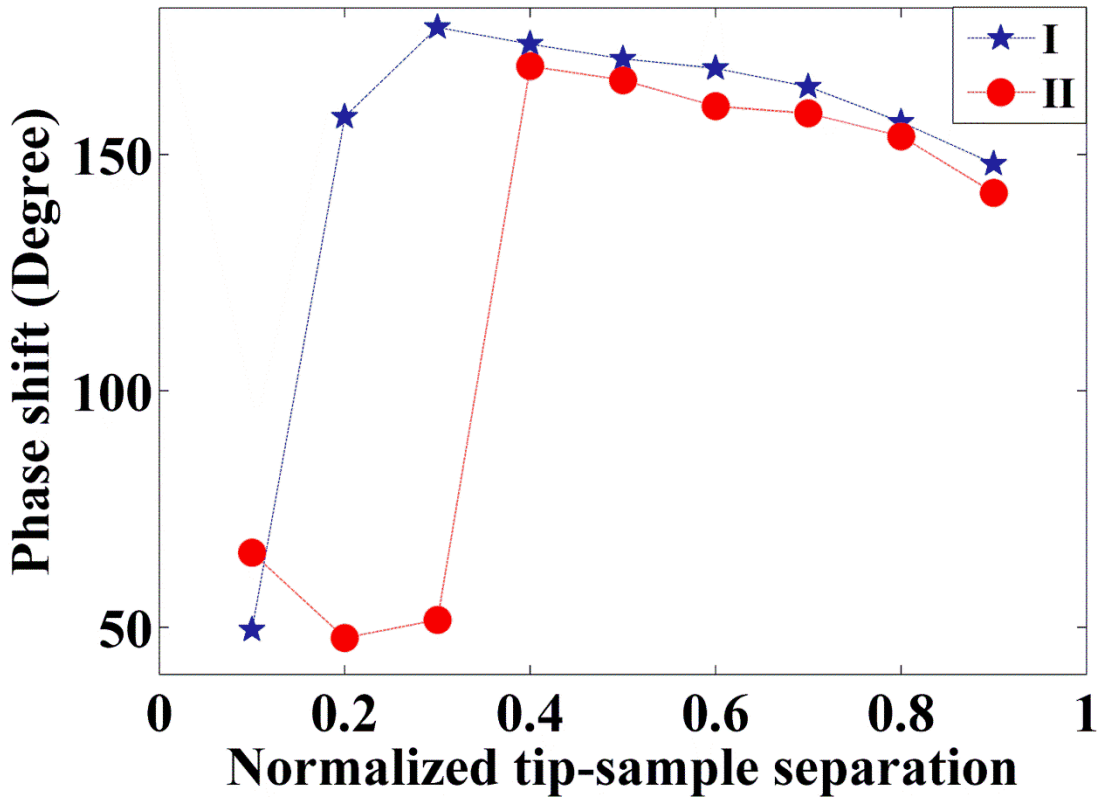

Figure 10 Phase shifts under elastic force with Young's modulus of 1GPa and Poisson's ratio of 0.4 coupled with I: adhesion hysteresis; II: adhesion hysteresis and van der Waals force. The $\gamma_{approach}$ surface energy is 30mJ/m^2 , the $\gamma_{retract}$ is 90mJ/m^2 , the Hamaker constant is 6e-20 J. (Colour version: web only)

In order to verify whether modelling other attractive interaction forces has the ability to decrease the level of phase shift, the van der Waals force was also added. The results are shown in Figure 10. In Figure 10, curve I is adopted from curve III in Figure 9. Based on curve I, van der Waals force is further added by using Equations 6-8 to produce curve II, where the Hamaker constant is 6e-20 J and the surface energy γ is 30mJ/m^2. From Figure 10, it can be seen that the adding of the van der Waals force further decreases the phase shift. The transition from the repulsive regime to the attractive regime moves to larger tip-sample separations. While curve I approaches the attractive regime at a normalized tip-sample separation of 0.1, curve II approaches to the attractive regime at a normalized tip-sample separation of 0.3, which once again demonstrates the contribution made by the repulsive and attractive forces shown in Figure 8. It can be noticed that the phase shift suddenly increases at a normalized tip-sample separation of 0.1, which could possibly be due to the strength of the attractive force somehow becoming weaker, but the overall interaction force is still attractive.

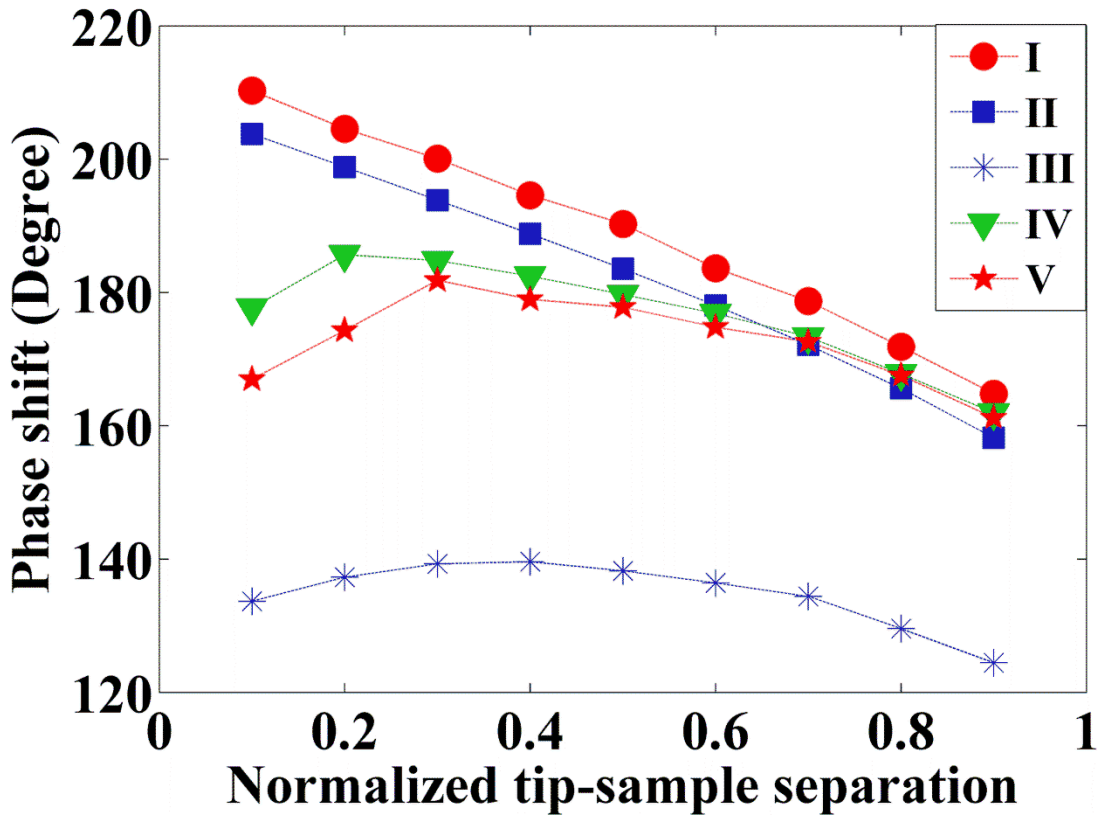

Figure 11 Phase shifts under elastic force and for different viscosity forces. I: elastic force only; II: elastic force + low viscosity force. III: low viscosity force only; IV: elastic force + high viscosity force. V: high viscosity force only. (Colour version: web only)

Figure 11 shows the simulated behaviour of the cantilever phase shifts when elastic and viscosity forces are applied to the cantilever tip in the Z-axis. The elastic force is defined here with a Young's modulus of 1GPa and a Poisson's ratio 0.4, by using Equation 1. The low viscosity force is calculated based on a viscosity of 500Pa*s by using Equation 5, while the high viscosity force is calculated based on a viscosity of 5000Pa*s. For curve I, only the elastic force is applied to the cantilever tip. For curve II, a low viscosity force and the elastic force are both applied to the tip. Comparing curves I and II, it can be seen that the added viscosity forces cause around 6^{o} of phase shift at every point of normalised tip-sample separation. Curves III and V show the phase shifts when only the viscosity force is applied. From curves III and V, when we have only viscosity force applied, it can be seen that the phase shifts both decrease when the tip approaches the sample. Curve IV, shows a situation where a high viscosity force and the same elastic force that was used previously are both applied to the tip. From Figure 11, it can be seen that curve IV has a similar trend to curve III, which indicates that here the viscosity force is dominant. As the viscosity force consists of both a repulsive force and an attractive force, when the elastic force is included as in curve IV, the overall force becomes repulsive, thus the phase shifts are all above 90^{o}.

From Figures 9 and 11, it can be observed that a phase image obtained using a small tip-sample separation provides more information on the sample features, such as the elasticity, viscosity and adhesion of material, because at normalized tip-sample separations ranging from 0.1 to 0.3, the phase shifts under different interaction forces can be differentiated.

The results shown above have been produced using the same elastic force with a Young's modulus of 1 GPa and a Poisson's ratio of 0.4. In order to investigate how phase shifts change under different elastic forces, simulations were also performed by changing the Young's modulus value to 5 GPa. The results are presented in Figure 12.

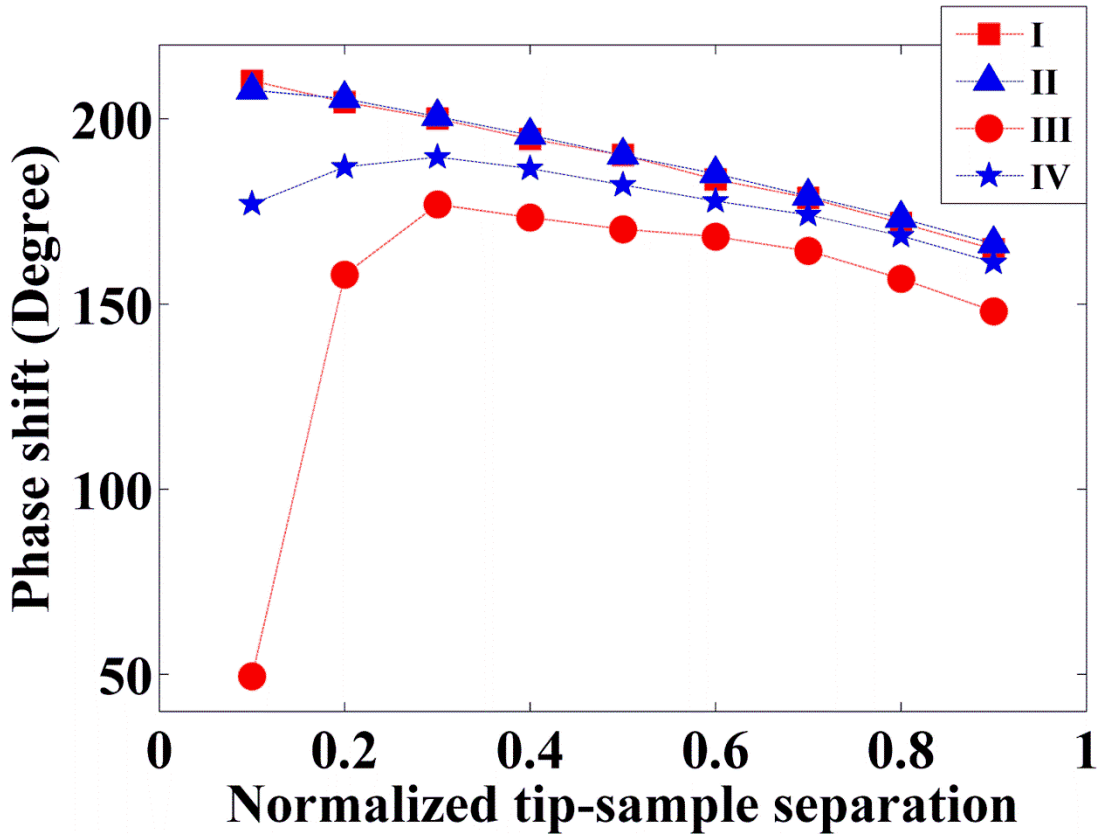

Figure 12 Phase shifts of I: only elastic force with a Young's modulus of 1GPa and Poisson's ratio of 0.4; II: only elastic force with a Young's modulus of 5GPa and Poisson's ratio of 0.4; III , IV are based on I and II, respectively, with the same adhesion hysteresis, where the $\gamma_{approach}$ surface energy is 30mJ/m^2 and the $\gamma_{retract}$ is 90mJ/m^2. (Colour version: web only)

In curves I and II of Figure 12 we are only considering the elastic force on the cantilever tip's surface in the Z-axis, with two different Young's moduli of 1GPa and 5GPa, respectively, and Poisson's ratios of 0.4. It can be seen from the figure that these two curves almost overlap each other. Thus, this indicates that the phase shifts are not sensitive to a change of Young's modulus in the case of purely elastic force existing. Curves III and IV show the behaviour of the phase shifts when adhesion hysteresis is coupled into curves I and II, where the approaching surface energy $\gamma_{approach}$ is 30mJ/m^2 and the $\gamma_{retract}$ is 90mJ/m^2. Curve IV is under the repulsive regime at all tip sample separations, because the strength of the elastic force is dominant. From curves III and IV, it is observed that the elastic force does affect the phase shifts in the case of combined forces applied to the tips, which always happens in real AFM experiments.

4.3 Transition time

Here, the transition time is calculated when the amplitude of the cantilever has reached the pseudo stable amplitude~~, which will be discussed in the next section.~~ The pseudo stable amplitude is defined in this paper for the convenience of analysis as the case when the difference of the amplitude between a current vibration cycle and the previous vibration cycle is smaller than 1nm. The pseudo stable amplitude is calculated from the displacement signal below zero as shown in Figure 4. The transition time taken to move from Zone I to Zone III, as shown in Figure ~~3~~4, limits the AFM scanning speed. Therefore, an investigation of the transition times under different conditions, such as different tip-sample interaction forces and different tip-sample separations, can provide guidance on the selection of the optimal scanning speed to use in tapping mode AFM imaging.

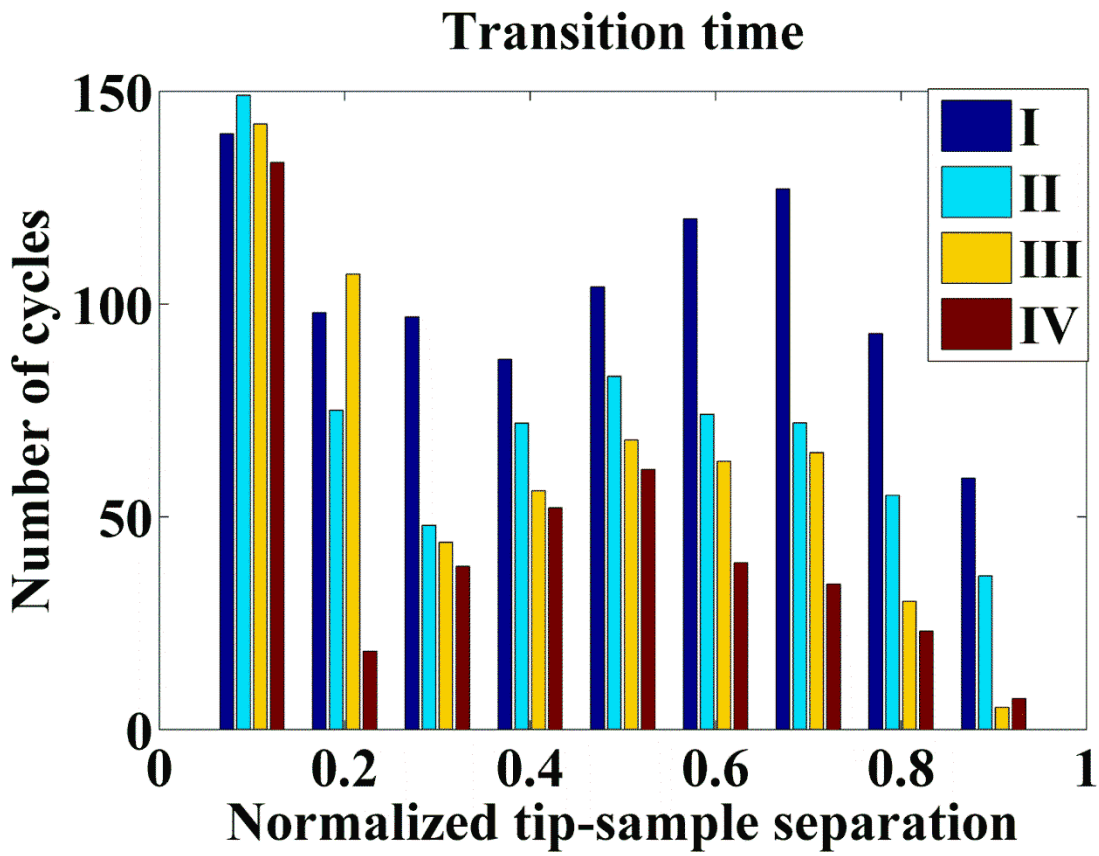

Figure 13 Transition time: I. purely elastic force. II, III, IV. elastic force and different levels of adhesion hysteresis. For II, III and IV, the $\gamma_{approach}$ is 30mJ/m^2; The $\gamma_{retract}$ is, 35mJ/m^2 (II), 60mJ/m^2 (III), 90mJ/m^2 (IV) respectively. (Colour version: web only)

Figure 13 shows the transition time calculated from the simulated dynamic displacement responses used to obtain the phase shifts presented in Figure 9. Since a virtual driving

sinusoidal voltage with a frequency of 62,920Hz is applied to the virtual piezo actuator to vibrate the cantilever, the period of the driving voltage is 1.5893e-5 seconds. In Figure 13, the transition time is expressed as a number of cycles which is based on the period of this driving voltage. The transition time is the vibration time of Zone II which is marked upon the dynamic displacement response shown in Figure ~~3~~4.

From Figure 13, it can be seen that the transition time is relatively short at normalized tip-sample separation around 0.2 or 0.9. However, either case may result in losing the contribution from the elasticity or adhesion of the material as shown in Figure 9. At a normalized tip-sample separation of 0.2, the phase shifts are below 90^0, which indicate that attractive forces are dominant. On the other hand, repulsive forces are dominant at a normalized tip-sample separation of 0.2. Thus, in order to capture a phase image with the contributions from both elasticity and adhesion, we may need to compromise the scanning speed by choosing a normalized tip-sample separation around 0.4, because the phase shifts are about to change from repulsive regime to attractive regime as shown in Figure 9, which contain the contributions from repulsive force and attractive force.

4.4 Vibration period in each cycle

Phase shifts are due to shifts in the cantilever's resonant frequency. Without any tip-sample interactions, the phase shift corresponding to the resonant frequency would be 90^0. It was found that the phase shift would become smaller than 90^0 for small tip-sample separations, while the resonant frequency of the cantilever would shift to higher frequencies. For relatively large tip-sample separations, the phase shift would be larger than 90^0, while the resonant frequency would shift to lower frequencies (Magonov et al., 1997). Figure 16 shows the vibration periods of each vibration cycle in a simulated dynamic displacement response signal. The simulated dynamic displacement response signal is obtained under the conditions: Young's modulus of 1GPa and Poisson's ratio of 0.4, approach surface energy $\gamma_{approach}$ is $30mJ/m^2$, and retract surface energies $\gamma_{retract}$ are $90mJ/m^2$.The vibration period is computed through a zero crossing method. The vibration period change in a cycle is equivalent to the frequency change in that cycle. From Figure 16, it can be seen that the period decreases during the transition stage of Zone II. The vibration period is the same both in Zone I and Zone III. The relationship between this dynamic behaviour and the phase shift is worthy of further study in the future.

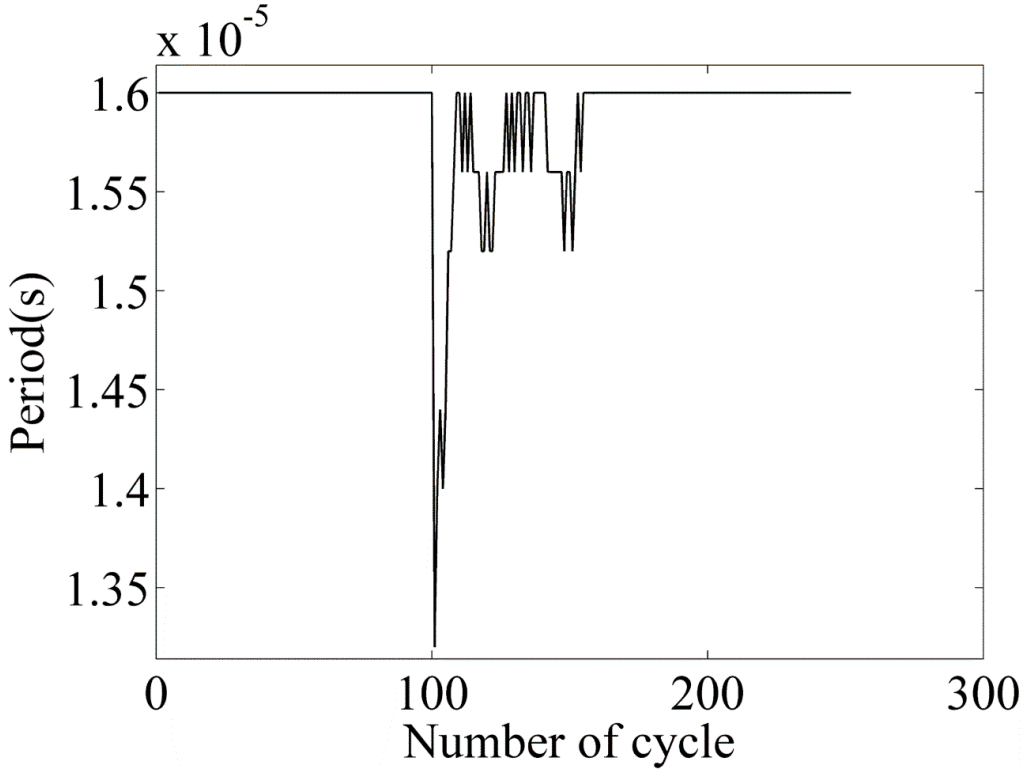

Figure 14 Vibration periods, Q=100, free vibration amplitude Amp_{free}= 40nm, tip-sample separation d0= 20nm. Young's modulus = 1GPa, Poisson's ratio = 0.4. $\gamma_{approach}$ = 30mJ/m^2, $\gamma_{retract}$ = 90mJ/m^2. Elastic force has been coupled with adhesion hysteresis to produce this result.

4.5 Discussions

We find that the simulation results obtained here could be a potential indicator on how to carry out real AFM experiments, which are summarized below:

- Phase trajectories shows that the dynamic behaviour of tapping mode is very complicated, which may be related to the tip-sample interaction forces and initial tip-sample separation. Further investigation may help understand the dynamic system of tapping mode AFM.
- Simulation results show that phase shifts caused by different adhesion energy hysteresis can be obviously separated under small normalized tip-sample separation. Therefore, in the aspect of AFM experiment, when surface energies and viscosity of the materials are known, small setpoint amplitude should be selected for scanning AFM images to obtain better phase contrast between different materials.
- Also, phase shifts caused by different viscosity can be obviously separated under small normalized tip-sample separation, which indicate that small setpoint amplitude should be chosen for AFM imaging.

- Simulation results also show that transition time is relatively shorter under small or large normalized tip-sample separation. This could be regarded as an indicator to optimize the scanning speed, during experiment, we should select either small or large setpoint amplitudes for AFM imaging, determined by taking into account what kind of surface propertied are of interest.

Instantaneous frequency shows that the frequency in each vibration cycle rapidly changes during the transition zone. Further study of this behaviour may help to investigate the origin of the phase shift.

5. Experimentation in support of the simulations

5.1 Atomic force microscopy set-up

In order to validate the simulated results, experiments were carried out using a Molecular Force Probe-3D (MFP-3D) atomic force microscope (Asylum Research, Santa Barbara, CA) with software written in IGOR pro (Wavemetrics, USA). The MFP-3D is equipped with a 90 μm x–y scanning range, z-piezo range > 16 μm and was coupled to an Olympus IX50 inverted optical (IO) microscope. The MFP-3D-IO was placed upon a TS-150 active vibration isolation table (HWL Scientific instruments GmbH, Germany), which was located inside an acoustic isolation enclosure (IGAM mbH, Germany) to help eliminate external noise. Silicon nitride cantilevers (Olympus model AC240TS) were used with nominal manufacturer values for length, width, thickness and tip radius of 240μm, 30μm, 2.7μm and 9nm respectively. Resonant frequency and spring constant (k) were measured at approximately 72 kHz and 2N/m, respectively.

5.2 Preparation of samples

For the experimental work two relatively soft samples, polyurethane (PU) and polyvinyl chloride (PVC), were used. The polymer was supplied by Biomer Technology Ltd in a liquid form. To develop the polymer the polyurethane solution was first poured into a glass petri dish and swirled until the polyurethane solution had contacted the edges of the glass dish. The polyurethane was then cured in the oven at 60˚C for 2 hours. The PVC was purchased commercially in the form of cling wrap. To prepare the samples ready for AFM the PU and PVC were placed securely on a glass microscope slide.

5.3 Cantilever calibration and AFM measurements

Experiments were performed using tapping mode AFM in air. Before experiments were carried out the cantilever was calibrated. This was achieved by characterising the inverse optical lever sensitivity (*Invols)*, which is software driven for the MFP3D AFM and is described in (Meyer and Amer, 1988). Cantilever calibration determined that an amplitude of

1 volt, as recorded by the photodetector, was equal to a cantilever displacement distance of 43.6nm.

For AFM measurements the cantilever was driven at its fundamental frequency (approx.72kHz) and ramped down until the setpoint amplitude was reached. Phase shifts were recorded by changing the setpoint ratio (setpoint ratio = setpoint amplitude/free amplitude). The phase shifts were recorded from set-point amplitudes varying from 900mV to 100mV. Data was recorded using the AFM software and analysed using Matlab. Efforts have also been made to capture the cantilever displacement response signal. However, owing to the limitations of oscilloscopes we have only captured the signal during contact. It is worth investigating further in future work.

5.4 Experimental results

For polyurethane (PU) and polyvinyl chloride (PVC), the phase shifts shown are in the repulsive regime. The phase shifts gradually increase when the tip sample separation decreases, which has a similar trend to that of the simulation results. The experiments were carried out over a total of 10 consecutive repetitions and we obtained similar results in all cases, which indicates that they could be used to support the findings of the simulation results.

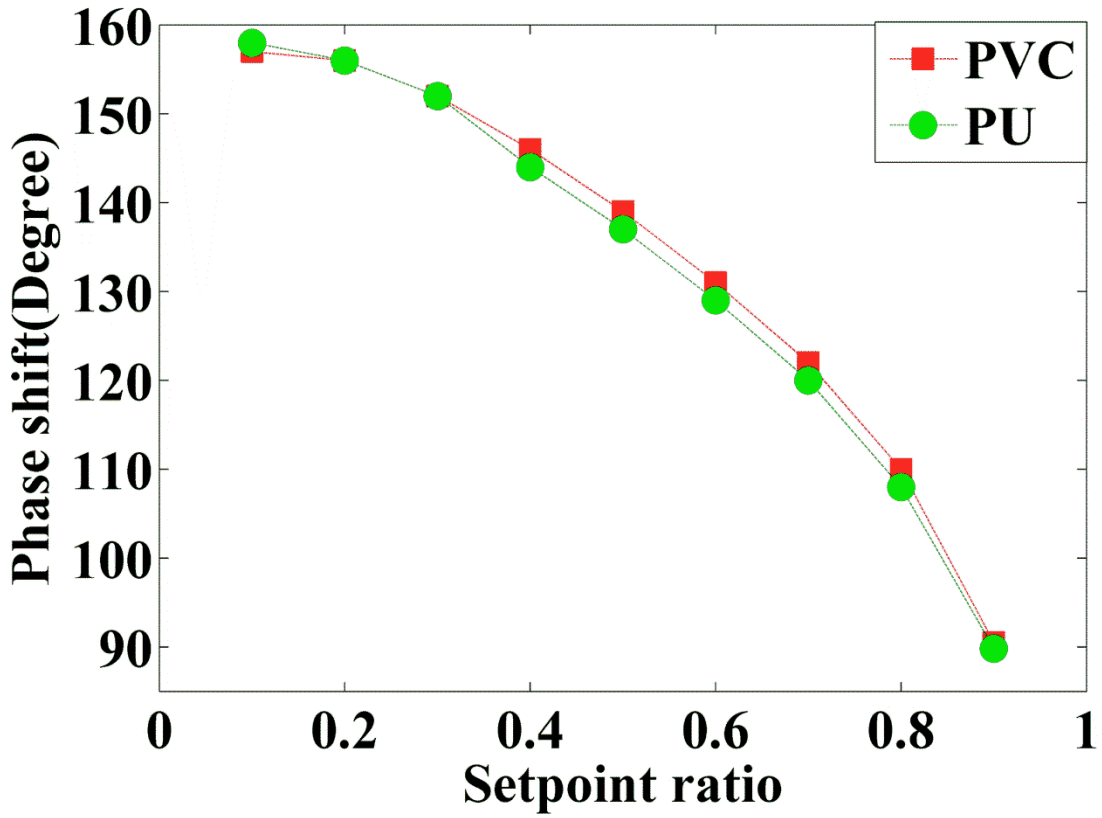

Figure 15 Experimental results for simulation validation. Q=154, free amplitude: 43.6nm, test sample: PVC, PU. (Colour version: web only)

6. Conclusions and ~~discussions~~ Future Work

A three dimensional finite element method has been proposed to study the cantilever's dynamic behaviour in tapping mode AFM. The cantilever's dynamic displacement responses under different tip-sample separations and for different tip-sample interaction forces, such as the elastic force, adhesion force, viscosity force and van der Waals force, have been studied through finite element analysis. Simulated results show that the dynamic displacement response can be divided into three zones, which were not observed in other simulation studies. The dynamic displacement responses that were obtained were used to investigate the cantilever's dynamic behaviour, such as phase shift, transition time~~, pseudo stable amplitude,~~ and frequency changes. The major findings of this paper are summarized below:

- The phase trajectory shows that dynamic behaviour of cantilever is very complicated, especially in the transition zone.
- Phase shifts are below 90^{o} when only attractive forces are considered. On the other hand, phase shifts are above 90^{o} when only repulsive forces are considered.
- When different interaction forces are coupled together, it was found that attractive forces, such as adhesion force and van der Waals force, have the ability to decrease

the phase shifts.

- Simulation results also provide potential guidance on how to perform AFM imaging.
- The proposed method provides a credible tool that can be used to interpret AFM phase images.

Experiments on a real AFM instrument were also carried out to support the findings of the simulations. However, there is a lot which can be done in the future.

- How to use dynamic behaviour to quantitatively interpret phase images still requires further study.
- In addition, within this paper we have only investigated the impact of the test samples reflected by the interaction forces on the dynamic behaviour of the cantilever.
- The impact of the shape, size and material properties of the AFM cantilever and tip upon the cantilever's dynamic behaviour will be studied in the future.
- Also, further investigation into interaction forces in the x and y directions will be considered in the future, as only interaction forces in the z direction are discussed here.
- The results that have been presented here help in understanding the vibration mechanism of the cantilever under various tip-sample interactions and may enable optimisation of system parameters to increase the quality of AFM phase images.
- This method also opens up an approach by which it is possible to investigate the dynamic behaviour of AFM cantilevers operating under other vibration modes, for example the second flexural mode.

Acknowledgement

This research leading to these results was carried out in General Engineering Research

Institute, receiving financial support from Liverpool John Moores University. Also, I would like to thank Biomer Technology Ltd (BTL) for providing test samples.

References

BAHRAMI, A. & NAYFEH, A. H. 2013. Nonlinear dynamics of tapping mode atomic force microscopy in the bistable phase. *Communications in Nonlinear Science and Numerical Simulation,* 18**,** 799-810.
BUYUKKOSE, S., OKUR, S. & AYGUN, G. 2009. Local oxidation nanolithography on Hf thin films using atomic force microscopy (AFM). *Journal of Physics D: Applied Physics,* 42**,** 105302.
DIAO, Y., TEE, B. C. K., GIRI, G., XU, J., KIM, D. H., BECERRIL, H. A., STOLTENBERG, R. M., LEE, T. H., XUE, G., MANNSFELD, S. C. B. & BAO, Z. 2013. Solution coating of large-area organic semiconductor thin films with aligned single-crystalline domains. *Nat Mater,* 12**,** 665-671.
DUVIGNEAU, J., KUTNYANSZKY, E., PHANG, I. Y., CHUNG, H.-J., WU, H., DOS RAMOS, L., GÄDT, T., YUSOFF, S. F. M., HEMPENIUS, M. A., MANNERS, I. & VANCSO, G. J. 2014. Raft crystals of poly(isoprene)-block-poly(ferrocenyldimethylsilane) and their surface wetting behavior during melting as observed by AFM and NanoTA. *Polymer,* 55**,** 2716-2724.
GARCÍA GARCÍA, R., SAN PAULO, Á. & TAMAYO, J. 1999. Phase contrast and surface energy hysteresis in tapping mode scanning force microscopy. *Surface and Interface Analysis,* 316**,** 312-316.
GARCIA, R., GÓMEZ, C., MARTINEZ, N., PATIL, S., DIETZ, C. & MAGERLE, R. 2006. Identification of Nanoscale Dissipation Processes by Dynamic Atomic Force Microscopy. *Physical Review Letters,* 97.
GARCÍA, R., TAMAYO, J., CALLEJA, M. & GARCÍA, F. 1998. Phase contrast in tapping-mode scanning force microscopy. *Applied Physics A,* 66**,** S309-S312.
JALILI, N. & LAXMINARAYANA, K. 2004. A review of atomic force microscopy imaging systems: application to molecular metrology and biological sciences. *Mechatronics,* 14**,** 907-945.
KASAS, S., LONGO, G. & DIETLER, G. 2013. Mechanical properties of biological specimens explored by atomic force microscopy. *Journal of Physics D: Applied Physics,* 46**,** 133001.
LIU, M. & GORMAN, D. G. 1995. Formulation of Rayleigh damping and its extensions. *Computers & Structures,* 57**,** 277-285.
MAGONOV, S. N., ELINGS, V. & WHANGBO, M. H. 1997. Phase imaging and stiffness in tapping-mode atomic force microscopy. *Surface Science,* 375**,** L385-L391.
MELCHER, J., HU, S. & RAMAN, A. 2008. Invited Article: VEDA: A web-based virtual environment for dynamic atomic force microscopy. *Review of Scientific Instruments,* 79**,** 061301.
MEYER, G. & AMER, N. M. 1988. Novel optical approach to atomic force microscopy. *Applied Physics Letters,* 53**,** 1045-1047.
PISHKENARI, H. N., MAHBOOBI, S. H. & MEGHDARI, A. 2011. Simulation of imaging in tapping-mode atomic-force microscopy: a comparison amongst a variety of approaches. *Journal of Physics D: Applied Physics,* 44**,** 075303.
SONG, Y. & BHUSHAN, B. 2006. Simulation of dynamic modes of atomic force microscopy using a 3D finite element model. *Ultramicroscopy,* 106**,** 847-873.
SONG, Y. & BHUSHAN, B. 2008. Atomic force microscopy dynamic modes: modeling and applications. *Journal of Physics: Condensed Matter,* 20**,** 225012.
TAMAYO, J. & GARCÍA, R. 1996. Deformation, Contact Time, and Phase Contrast in Tapping Mode Scanning Force Microscopy. *Langmuir,* 12**,** 4430-4435.
TAMAYO, J. & GARCíA, R. 1997. Effects of elastic and inelastic interactions on phase contrast images in tapping-mode scanning force microscopy. *Applied Physics Letters,* 71**,** 2394-2396.
WANG, Y., SONG, R., LI, Y. & SHEN, J. 2003. Understanding tapping-mode atomic force microscopy data on the surface of soft block copolymers. *Surface Science,* 530**,** 136-148.
WHITED, A. M. & PARK, P. S. H. 2014. Atomic force microscopy: A multifaceted tool to study membrane proteins and their interactions with ligands. *Biochimica et Biophysica Acta (BBA) - Biomembranes,* 1838**,** 56-68.

Figure captions